Open Channel Flow over a Pair of Rectangular Cylinders at Incidence

J.M. Tsikata, M. Agelinchaab, M.F. Tachie
Department of Mechanical Engineering, University of Manitoba, Winnipeg, Canada

1. Introduction

Fluid flows around cylinders are encountered in diverse engineering applications, as well as offshore and environmental settings. Examples include tall buildings and structures such as bridges, chimneys, trash racks for hydraulic turbines, cooling towers and heat exchangers. In this work, an experimental investigation was conducted using particle image velocimetry to study the mean flow and turbulence characteristics around a pair of rectangular cylinders in an open channel. The measurements were obtained at different streamwise-spanwise planes over and downstream of the cylinders to study the effects of cylinder pair angles of incidence on the flow field. The rectangular cylinders have thickness (D = 12 mm) to length (L = 100 mm) ratio of L/D = 8.3. The cylinder height was H = 190 and the centre-to-centre spacing between the cylinders is b = 51 mm. The experiments were performed for the following four angles of incidence: δ = 0°, 7.5°, 15.0°, and 22.5°.

2. Experimental Set-up and Measurement Procedure

The experiments were performed in an open water channel with a test section having dimensions of 2500 mm long, 200 mm wide and 200 mm deep. Figure 1 shows schematic side and plan views of the test section with the cylinder pair assembly. The cylinders were mounted vertically in the channel. The figure also serves to define some of the flow nomenclature and the coordinate system adopted. Note that x = 0 is at the trailing edge of the cylinder.

The flow was seeded with 5 μm polyamide seeding particles that have a specific gravity of 1.03. An Nd-YAG, 120 mJ/pulse laser of 532 nm wavelength was used to illuminate the flow field. The laser sheet was located at a distance y = 70 mm above the channel floor. A 12-bit high-resolution digital camera that uses a CCD with 2048 pixels × 2048 pixels and has a 7.4 μm pixel pitch was used to image the flow. To achieve adequate spatial resolution in the measurement, two different x-z planes were used to image each cylinder pair. The instantaneous images were processed using 32 pixels × 32 pixels interrogation window with 50% overlap and 1500 instantaneous image pairs were used to calculate the mean and turbulent statistics.

2. Preliminary Results

2.1 Flow Qualification: Prior to conducting measurements around and downstream of the cylinder, measurements were obtained at x/D = -35 to characterize the approach flow. The approach freestream velocity and depth of flow were maintained at U_e = 0.385 m/s and h = 140 mm, respectively. The corresponding Reynolds number ($Re_s = U_eD/\nu$) and Froude number ($F = U_e/[gh]^{0.5}$) are 4620 and 0.33, respectively. The approach flow was, therefore, in turbulent and sub-critical regimes. The mean streamwise velocity distributions and turbulent intensity of the approach flow are shown in Fig. 2. The background turbulence level close to the free surface was u/U_e = 0.08 which is an order of magnitude higher than typical values reported in wind tunnel experiments. It was observed that the approach flow was substantially distorted by the presence of the cylinder pair, and the degree of distortion varied with the angle of incidence. Figure 2c shows the dip in the free surface close to the cylinder pair (relative to the undisturbed free surface). The dips generally increase with angle of incidence.

2.2 Mean velocity and turbulent quantities along the wake axis: Fig. 3 shows the effects of incidence angles on the profiles of the streamwise mean velocity and turbulent quantities along the wake centerline. At δ = 0°, the recirculation lengths (l_r) of the cylinder at top (above) and the one at the bottom (below) are similar. As δ increases, l_r values for the cylinder above and the one below both decrease. However, the values below decrease at such a faster rate that at δ = 22.5°, l_r = 0 (*i.e.*, no recirculation). The peaks of the streamwise turbulent intensities increase with δ but the profile above are higher than those below. The Reynolds shear stresses are very small (closed zero) with the exception of δ = 22.5°.

2.3 Streamlines and iso-contours: The iso-contours of the mean velocity, and Reynolds shear stress for δ = 0.0° to 22.5° are shown in Figs. 3 and 4. In each plot, the mean streamlines are shown to reveal the mean flow pattern. Two different planes were used to image the cylinders and laid out side by side. An arrow '↓' is used to indicate the point of contact of the two planes. The mean flow separated near the leading edge of the cylinder pair and a pair of counter rotating vortices of nearly similar sizes and intensities are formed downstream the trailing edges of cylinder at δ = 0.0°.

As incidence angle is increased to δ = 22.5°, only anti-clockwise (lower) vortices were found at the trailing edges. It appears that the proximity of the cylinders to each other and to the channel wall annihilated the clockwise (upper) vortices. The iso-contours of the mean velocity show maximum velocities at the top and bottom side of the cylinders and minimum velocities at the wake region δ = 0.0°. More Reynolds shear stresses are produced as the angle of incidence increases. It is evident that the Reynolds shear stresses are much higher closed to the leeward side of the cylinders.

2.4 Mean velocity and turbulent quantities across the wake axis: The mean velocity profiles, turbulent intensities and Reynolds shear stress across the wakes axes at selected locations are shown in Fig. 5. Note that the profiles are staggered in the horizontal axis. At δ = 0° the mean velocity profiles are nearly symmetrical about z = 0. As δ increases, the mean velocities

increase and become increasingly asymmetric. The peak values of the turbulent intensities and Reynolds shear stresses also increase with δ.

3. Final Paper

The final paper will provide a comprehensive summary of prior studies and detailed description of the experimental set up and measurement procedure. Profiles of the mean velocities and turbulence statistics along and across the wakes axes will be discussed in more details in the context of prior studies. The physical insight as well as the comprehensive data sets obtained in this turbulent shear flow field will be very useful for validating future results from numerical simulations.

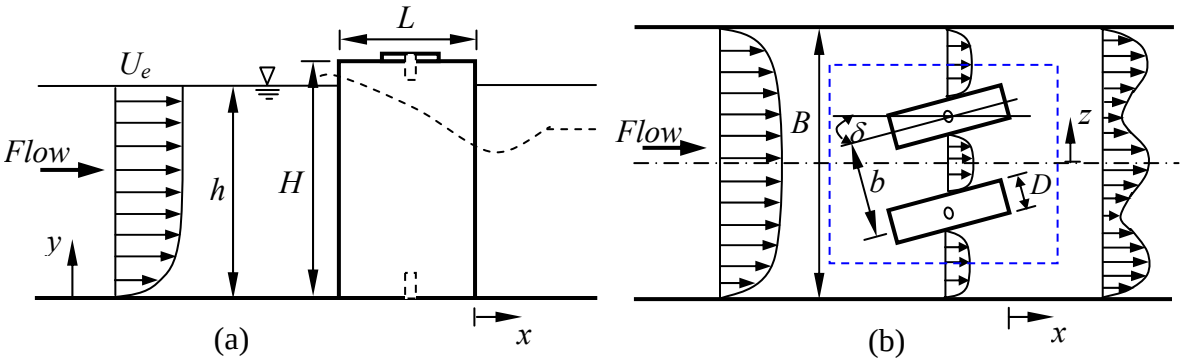

Fig. 1: Side (a) and plan (b) views of test section

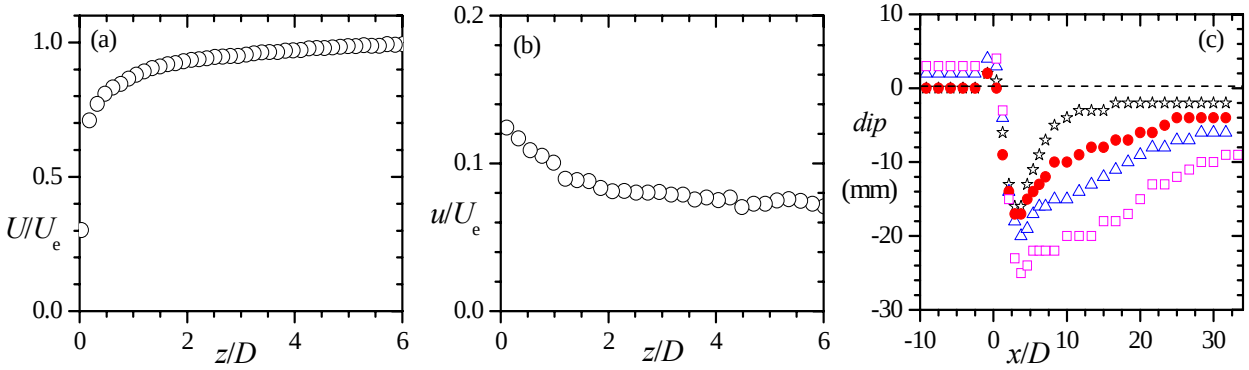

Fig. 2: Mean velocity distribution (a), streamwise turbulent intensity (b), and dip in the free surface close to the cylinders, (c). Symbols in (c): δ = 0.0° (☆), 7.5° (●) 15.0° (△) 22.5° (□).

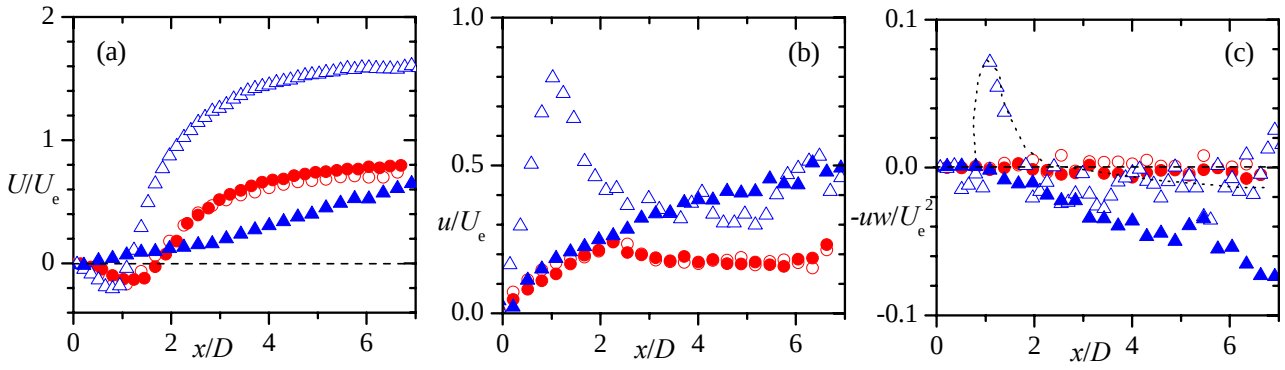

Fig. 3: Streamwise mean velocity distribution (a), turbulent intensity (b), and Reynolds shear stress along the wake axis for δ = 0.0° and 22.5°. Symbols: above δ = 0.0° (○), 22.5° (△); below δ = 0.0° (●), 22.5° (▲).

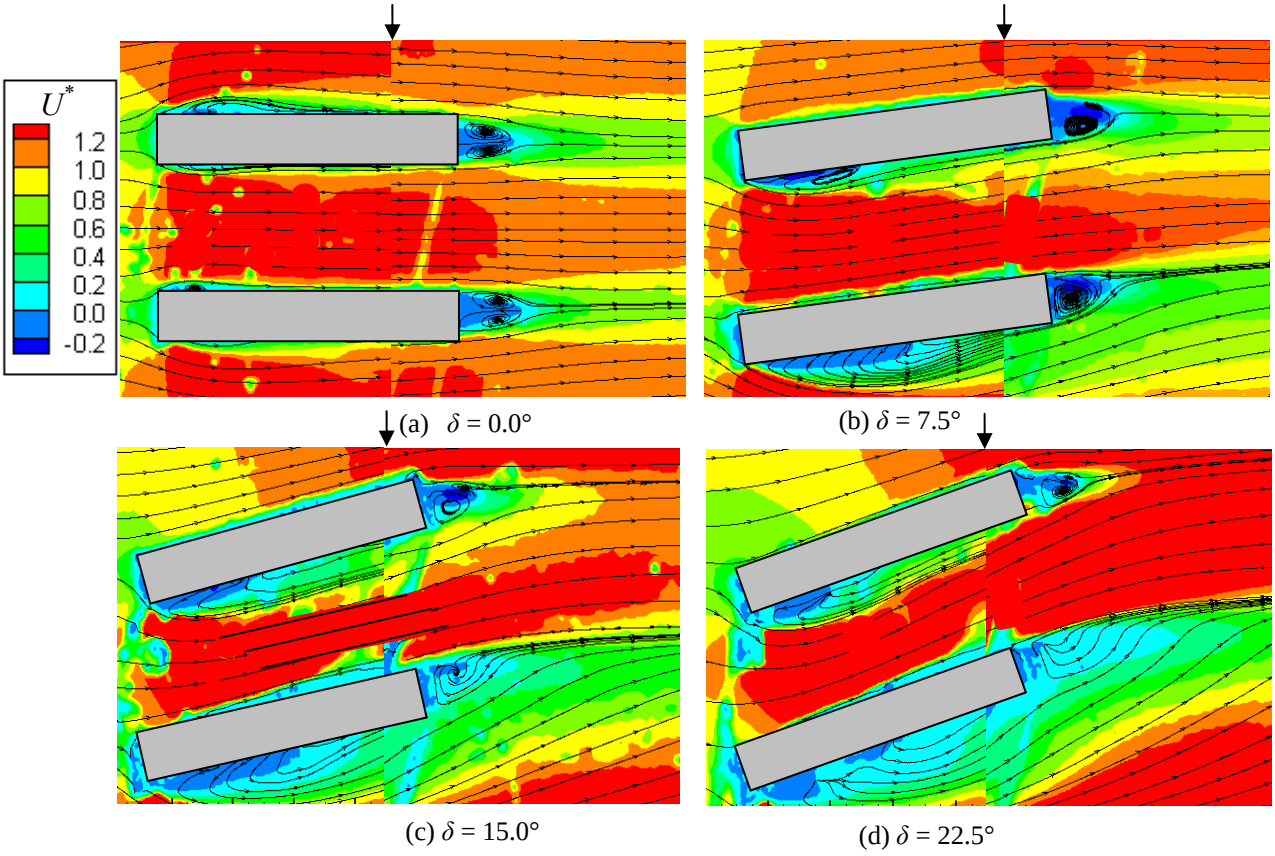

Fig. 4: Iso-contours of mean velocity ($U^* = U/U_e$) for incidence angles of δ = 0.0° (a), 7.5° (b) 15.0° (c) 22.5° (d).

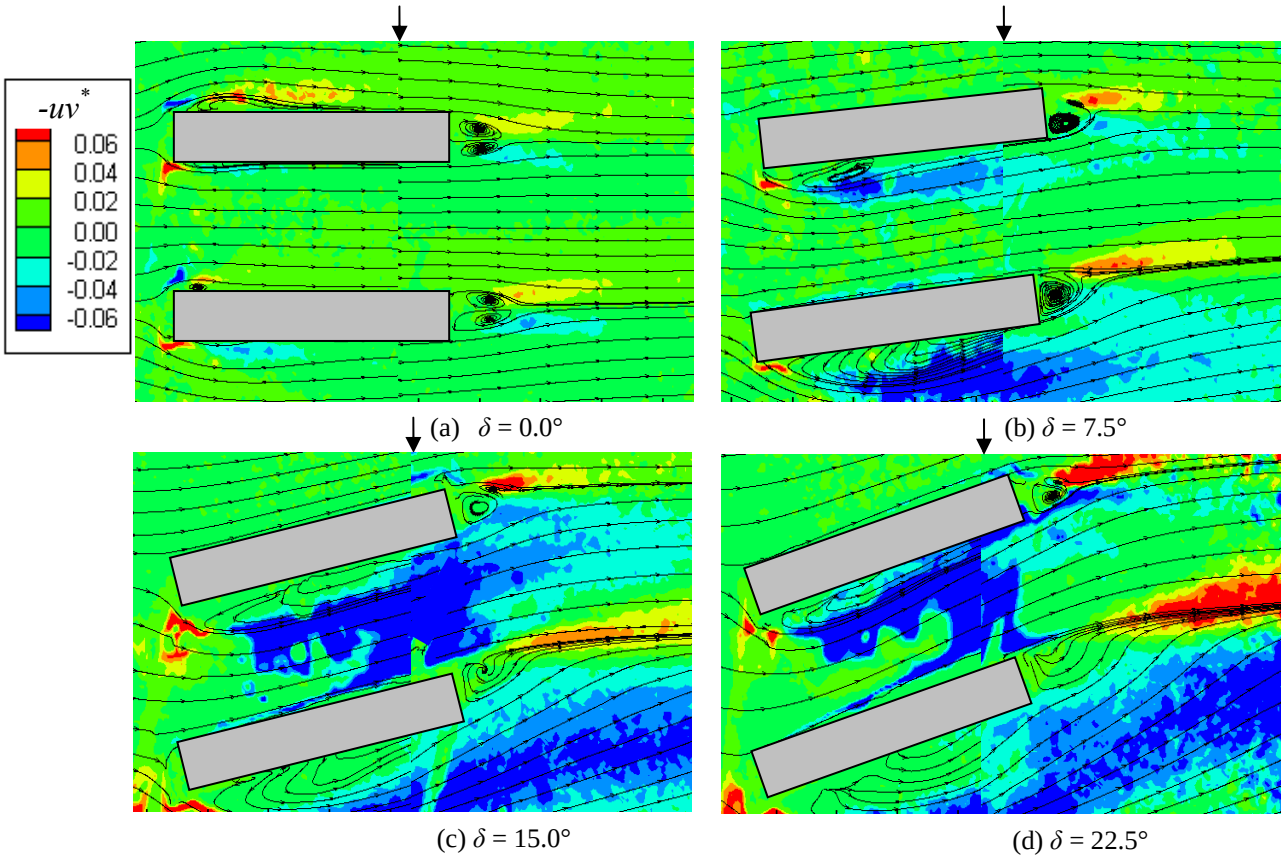

Fig. 5: Iso-contours of Reynolds shear stress ($uw^* = uw/U_e^2$) for incidence angles of δ = 0.0° (a), 7.5° (b) 15.0° (c) 22.5° (d).

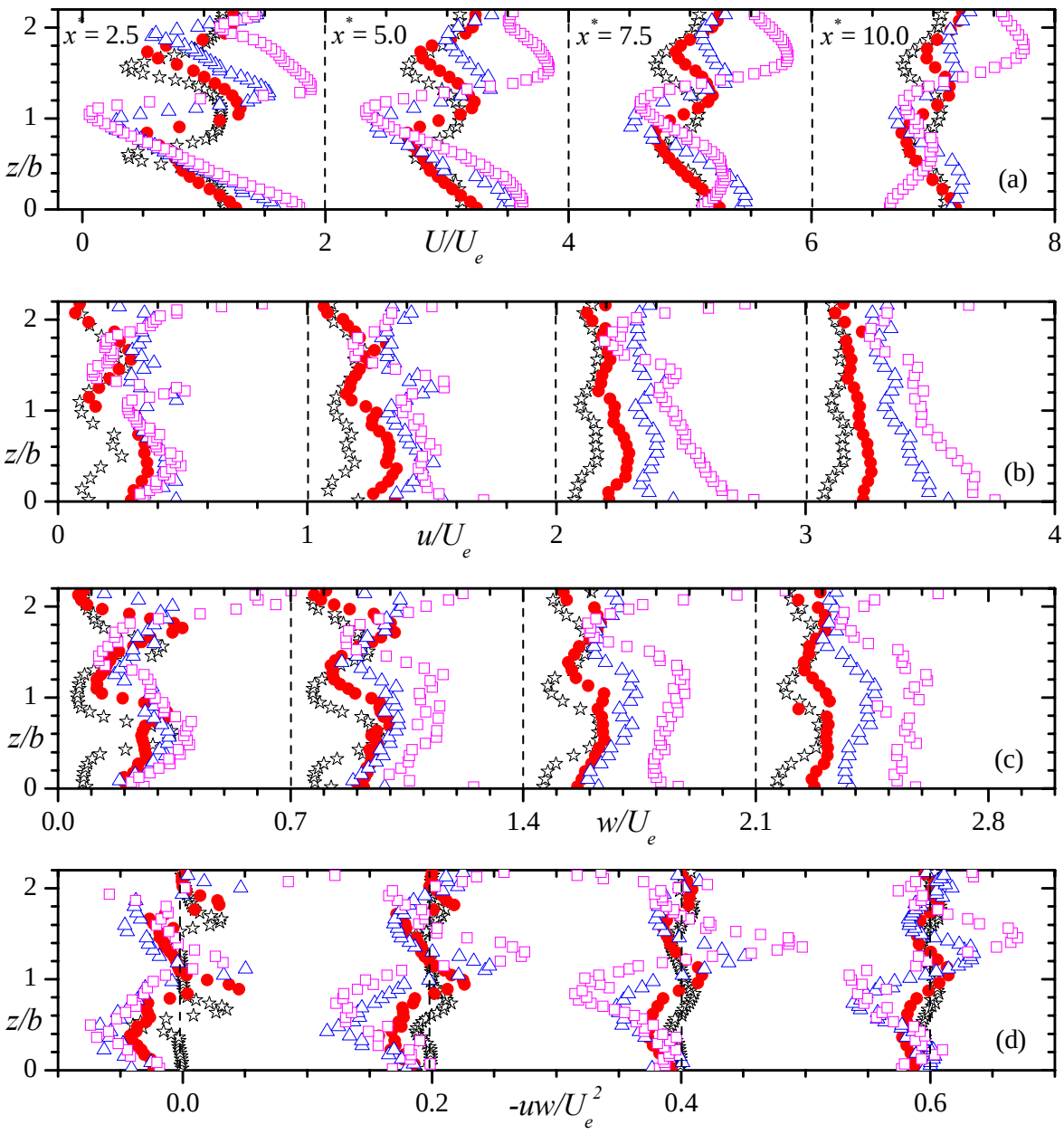

Fig. 6: Mean velocity and turbulent quantities at selected, $x^* = x/D$, locations (a) mean velocity, (b) streamwise , (c) spanwise turbulent intensities, and (d) Reynold shear stress. Symbols: δ = 0.0° (☆), 7.5° (●), 15.0° (△), and 22.5° (□). All x^* locations correspond to those in (a).